Astronomy
&
Astrophysics

SPI observations of the diffuse ^{60}Fe emission in the Galaxy

W. Wang[1], M. J. Harris[1], R. Diehl[1], H. Halloin[2], B. Cordier[4], A. W. Strong[1], K. Kretschmer[1], J. Knödlseder[3], P. Jean[3], G. G. Lichti[1], J. P. Roques[3], S. Schanne[4], A. von Kienlin[1], G. Weidenspointner[3], and C. Wunderer[5]

[1] Max-Planck-Institut für extraterrestrische Physik, Postfach 1603, 85740 Garching, Germany
   e-mail: wwang@mpe.mpg.de
[2] AstroParticule et Cosmologie (APC), 11 place Marcelin Berthelot, 75231 Paris, France
[3] Centre d'Étude Spatiale des Rayonnements, BP 4346, 31028 Toulouse Cedex 4, France
[4] DSM/DAPNIA/SAp, CEA Saclay, 91191 Gif-sur-Yvette, France
[5] Space Sciences Laboratory, UC Berkeley, CA 94720, USA

ABSTRACT

Aims. Gamma-ray line emission from radioactive decay of ^{60}Fe provides constraints on nucleosynthesis in massive stars and supernovae.
Methods. spectrometer SPI on board *INTEGRAL* has accumulated nearly three years of data on gamma-ray emission from the Galactic plane. We have analyzed these data with suitable instrumental-background models and sky distributions to produce high-resolution spectra of Galactic emission.
Results. We detect the γ-ray lines from ^{60}Fe decay at 1173 and 1333 keV, obtaining an improvement over our earlier measurement of both lines with now 4.9σ significance for the combination of the two lines. The average flux per line is $(4.4 \pm 0.9) \times 10^{-5}$ ph cm^{-2} s^{-1} rad^{-1} for the inner Galaxy region. Deriving the Galactic ^{26}Al gamma-ray line flux with using the same set of observations and analysis method, we determine the flux ratio of ^{60}Fe/^{26}Al gamma-rays as 0.148 ± 0.06.
Conclusions. The current theoretical predictions are consistent with our result. We discuss the implications of these results for the widely-held hypothesis that ^{60}Fe is synthesized in core-collapse supernovae, and also for the closely-related question of the precise origin of ^{26}Al in massive stars.

Key words. ISM: abundances – nuclear reactions, nucleosynthesis, abundances – gamma rays: observations

1. Introduction

The radioactive isotope ^{60}Fe is believed to be synthesized through successive neutron captures on Fe isotopes (e.g. ^{56}Fe) in a neutron-rich environment inside massive stars, before or during their final evolution to core collapse supernovae (CCSN). Due to its long decay time ($\tau \simeq 2.2$ My), ^{60}Fe survives to be detected after the supernova ejected it into the interstellar medium, by β-decay via ^{60}Co and γ emission at 1173 keV and 1333 keV – like other radioactive isotopes: ^{44}Ti, ^{56,57}Co, and ^{26}Al. These isotopes provide evidence that nucleosynthesis is ongoing in the Galaxy (with CCSN occurring at intervals $\sim$30−100 yr, The et al. 2006; Diehl et al. 2006). The discoveries of the above isotopes have fulfilled predictions of nucleosynthesis theory, at least in its general outline. The ^{44}Ti and ^{56,57}Co isotopes have relatively short half-lives ($\leq$100 years) and are thus detected as point-like sources, e.g. in young type II supernova remnants (SNRs) Cas A and 1987A, respectively (Iyudin et al. 1994, 1995; Matz et al. 1988; Kurfess et al. 1992). With its much longer half-life ($\sim$10^6 years), ^{26}Al may propagate over significant distances of $\simeq$few hundred pc, and accumulates in the interstellar medium (ISM) from many supernovae, until injection and β-decay are in balance in the ISM, giving rise to a diffuse and even Galaxy-wide glow (Mahoney et al. 1982; Prantzos & Diehl 1996). The behavior of ^{60}Fe from the same massive-star sources should follow that of ^{26}Al, since its half-life is similar, $\sim$2.2 $\times$ 10^6 years. In addition, ^{60}Fe could also be produced in substantial amounts

by rare subtypes of SN Ia (Woosley 1997), which would then be point sources of ^{60}Fe gamma-rays.

Although the detections of these isotopes are in agreement with the broad outlines of CCSN nucleosynthesis theory, there are discrepancies in the details. For example, ^{44}Ti lives long enough so that it should have been detected from several recent Galactic supernovae if these occur at a rate of $\sim$2 per century; but with the exception of Cas A (Iyudin et al. 1994; Renaud et al. 2004, 2006), no other SNRs have been detected yet. Mapping of the diffuse ^{26}Al emission (Knödlseder et al. 1999; Plüschke et al. 2001) confirms that it follows the overall Galactic massive star population, but concentrations of ^{26}Al are seen in very young OB associations where even the most massive stars are not expected to have exploded (e.g. Cygnus OB associations). This has led to the suggestion that most ^{26}Al production is associated with ejections in an earlier, pre-explosion phase of stellar evolution (Knödlseder et al. 1999).

Measurements of ^{60}Fe promise to provide new information about these issues, specifically the massive star nucleosynthesis in the late pre-supernova stages. RHESSI reported observations of the gamma-ray lines from ^{60}Fe with 2.6σ significance, and an average flux of $(3.6 \pm 1.4) \times 10^{-5}$ ph cm^{-2} s^{-1} (Smith 2004). The analysis of the first year of data from the SPI spectrometer on ESA's *INTEGRAL* spacecraft resulted in a similarly marginally-significant detection of these γ-ray lines from ^{60}Fe ($\sim$3σ, Harris et al. 2005), with an average line flux of $(3.7 \pm 1.1) \times 10^{-5}$ ph cm^{-2} s^{-1}. SPI on *INTEGRAL* has accumulated more data since then; here we analyzed 2.5 years of data,

aiming at a consolidation of the *INTEGRAL*/SPI measurement of ^{60}Fe gamma-rays.

In the following section, we describe our observations with SPI. In Sect. 3, we describe the steps and methods of data analysis. The scientific results, including the spectra and intensities of both 1173 keV and 1333 keV lines, and the flux ratio of ^{60}Fe/^{26}Al are presented in Sect. 4. Discussions and a summary follow in Sect. 5.

2. Observations

The *INTEGRAL* spacecraft was launched on October 17, 2002, into a high-inclination, high-eccentricity orbit intended to avoid the increased background from the Earth's trapped radiation belts. *INTEGRAL*'s orbital period is 3 days. The spectrometer SPI consists of 19 Ge detectors actively shielded by a BGO anti-coincidence shield. It has a tungsten coded mask in its aperture which allows imaging at ~3° resolution within a 16° × 16° full coded field of view (imaging on *INTEGRAL* is mainly performed at lower energies by the IBIS telescope, with which SPI is co-aligned). The Ge detectors are sensitive to gamma-rays between 15 keV and 8 MeV, with a total effective area ~70 cm^2 at 1 MeV, and achieve an energy resolution of ~2.5 keV at 1 MeV (Roques et al. 2003; Attié et al. 2003). However, cosmic-ray (CR) impacts degrade this resolution over time, and the instrument is periodically shut off for a few days while annealing (by heating from cryogenic temperatures to 100 °C) is applied to the detectors to restore the energy resolution by thermal curing heating of the CR-induced defects (Roques et al. 2003; Leleux et al. 2003).

In space operations, *INTEGRAL* with its IBIS and SPI telescopes is pointed at predesignated targets, with a fixed orientation for intervals of typically ~2000 s (referred to as *pointings*), which are successively arranged as a standard pattern of neighbouring pointings ≃2° apart (*dithering*), and covering target region of interest for improved imaging (Courvoisier et al. 2003).

The interval covered by the observations analyzed here is December 3, 2002–August 22, 2005 (orbits 17–359). The instrument was in operation for most of this time, but important gaps were caused by five of the annealing episodes described above, and by the regular perigee passages with gaps due to the radiation belts. The live time was further reduced by the failure of two of the 19 detectors during this interval (December 2003 and July 2004) and by the occurrences of solar flares.

3. Data analysis

The basic measurement of SPI consists of event messages per photon triggering the Ge detector camera. We distinguish events which trigger a single Ge detector element only (hereafter *single event*, SE), and events which trigger two Ge detector elements nearly simultaneously (hereafter *multiple event*, ME), which is the case for ≃30% of ^{60}Fe gamma-ray photons.

The analysis steps are: (1) Assembly of data selected to be free of contamination by, e.g., solar-flare events. (2) Modelling the instrumental background. (3) Fitting the measured data in narrow energy bins with the background model and a model of celestial gamma-ray emission, folded through the instrumental response into the data space of the measurement; the fitted amplitude of the celestial model per energy bin then comprises the spectrum of observed sky emission. (4) Deriving line parameters of the celestial signal. From the two event types, and from the two gamma-ray lines of ^{60}Fe, we obtain four independent measurements of ^{60}Fe emission.

In the following, we discuss the analysis steps and their implementation in the corresponding software utilities within MPE's *INTEGRAL* data analysis system.

3.1. Data selection and assembly

We test data quality per each "science window" (typically a time interval of ~30 min corresponding to one pointing), applying selection limits to "science housekeeping" parameters such as the count rates in several onboard radiation detectors, instrument status codes, data ownership, and orbit phase (utility *spiselectscw*). We employ the *INTEGRAL* Radiation Environment Monitor (IREM; Hajdas et al. 2003), the SPI plastic scintillator anticoincidence counter (PSAC), and the rate of saturating events in SPI's Ge detectors (from events depositing >8 MeV in a detector; hereafter referred to as GEDSAT rates) to exclude solar-flare events and other erratic background increases. Regular perigee background increases are additionally eliminated through a 0.05–0.95 window on orbital phase. From the selected events, spectra are accumulated per each detector and pointing, and together with dead time and pointing information assembled into the analysis database.

We establish databases of spectra per pointing per detector for single and multiple events (SE and ME), in spectral ranges with 1 keV bin size in ~20 keV bands around each of the ^{60}Fe lines, and in adjacent energy bands for determination of instrumental background (see below). Typical such raw data spectra around two γ-ray lines are presented in Fig. 1, and show that instrumental background including strong instrumental lines dominates the raw spectra. The energy ranges around the two lines extend from 1153–1193 keV and 1313–1359 keV. For the background modelling from the adjacent continuum, we use 1163–1169 keV plus 1177–1184 keV, and 1318–1328 keV plus 1336–1349 keV energy bands, respectively. From orbits 17 to 359, a total observation time of ~24 Ms is thus obtained, with a data set consisting of 14 623 pointings with one spectrum per each detector and event type.

3.2. Background modelling

SPI spectra are dominated by the intense background radiation characteristic of space platforms undergoing CR bombardment. Much of this radiation is prompt, resulting directly from CR impacts, whose variation with time ought to follow that of the incident CR flux. Other components arise from radioactive isotopes produced by the CR impacts, whose decay lifetimes are long compared to the coincidence window of the detector-anticoincidence electronics. Radioactive isotopes will increase in abundance until CR production balances β-decay. A time series of their γ-ray emission will be the convolution of the time behavior of the prompt CR source with an exponential decrease from decay. Local radioactivity in the spacecraft and instruments themselves thus will generate both broad continuum background emission and narrow gamma-ray lines from long-lived radioisotopes. Varying with energy, background components may exhibit complex time variability due to their origins from more than one physical source.

We derive models for the background contribution per energy bin and pointing in each detector from comparisons to presumed "tracers" of background; for these, we use independent contemporaneous measurements aboard *INTEGRAL* (see Halloin et al. 2007; Diehl et al. 2006; also background model studies by Sizun et al. 2007). Comparing different candidate
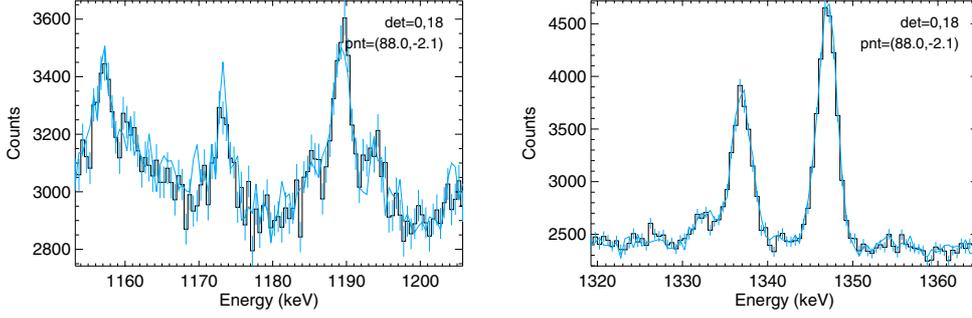
Fig. 1. Raw data spectra around the energies of two ^{60}Fe lines in one-INTEGRAL-orbit observations (3 days), representing the instrumental lines and continuum background. For the 1173 keV case (*left*), three strong instrumental lines are obvious: ^{44}Sc (1157 keV), ^{60}Co (1172.9 keV), ^{182}Ta (189.4 keV), and the ^{60}Co line blends with the ^{60}Fe line (Weidenspointner et al. 2003). For the 1333 keV case (*right*), the ^{60}Co background line (1332.5 keV) and the other strong instrumental line of ^{69}Ge (1336.8 keV) blend with the ^{60}Fe line, an instrumental line at 1347 keV also comes from ^{69}Ge electron captures.
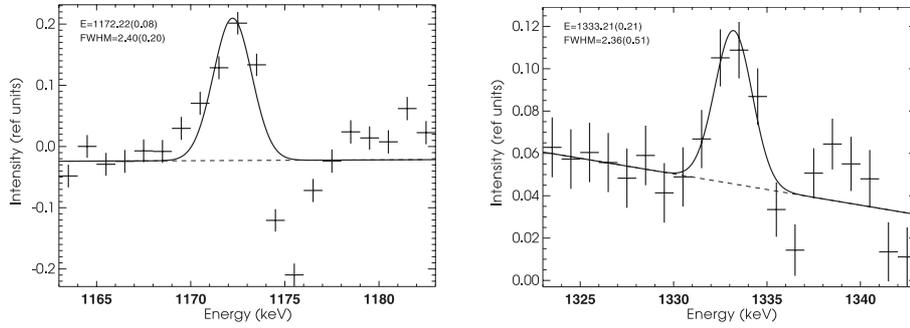

Fig. 2. Background coefficients for the ^{60}Co radioactivity build-up model around the 1173 keV (*left*) and 1333 keV (*right*) lines, respectively.

tracers to observed background variations, we find the best tracer(s) of background for each energy band. Candidate tracers with high statistical precision are the rates measured in SPI's plastic scintillator anticoincidence detector, the rate of saturated events in the BGO shield, the detector-by-detector GEDSAT rates (from events depositing >8 MeV in a Ge detector), and Ge-detector rates integrated over rather wide energy bands (for better statistical precision). For our analysis, we make use of the GEDSAT rates tracing the prompt CR activation to the ^{60}Fe lines (see above).

Each such tracer is regarded as a "template" for time variability of background. By normalizing such a template to the set of counts per detector spectrum (i.e. per pointing), a background model can be constructed, which is applicable to the analysis data set of spectra. We construct our background model from two components, one derived from adjacent energy bands, and an additional component modelling instrumental line contributions.

The most important radioactive background line component for our analysis is the emission from ^{60}Co decay inside the instrument, whose two lines at 1173 and 1333 keV are actually part of the celestial ^{60}Fe decay chain we want to measure. The convolution of the GEDSAT CR source tracer with an exponential function $e^{-t/\tau}$, in which the decay time τ is that of ^{60}Co (7.6 yr), is expected to give a good background model for energy bins containing contributions from these lines, i.e. around 1173 and 1333 keV (see Fig. 2). Another possible radioactive contaminant in our spectral region of interest may be the strong ^{69}Ge K-shell electron capture line (1337 keV, Weidenspointner et al. 2003) which blends into the 1333 keV ^{60}Fe line; its lifetime is 2.35 days. Because of the short decay time, we just take the

GEDSAT as a background component tracer for this strong instrumental line feature.

Thus, in a first step, the detector-by-detector count rates in the four continuum bands are fitted by the GEDSAT time series to construct an "adjacent-energies" background template. Then, the set of detector-by-detector spectra per pointing in 1 keV bins covering the ~20 keV intervals around and including the ^{60}Fe lines are fitted to the sum of adjacent continuum template, plus the radioactivity template for ^{60}Co, plus an additional GEDSAT template to capture any additional prompt background. Thus we generate a background model for our actual set of spectra, which is constrained in its variability by the various background tracers. Contributions of celestial gamma-ray events are small, their variability is intrinsically different due to the coded-mask modulation of the background model supplemented by dithering, and thus is expected only to affect global normalization, but not the variability with time.

We then orthogonalize the different background model components for an improved convergence of the fitting (also see Sect. 2.2 of Diehl et al. 2006; this step ensures that each higher-order background component carries new and independent information).

Representing our data sets with background-models only, we obtain reduced χ^2 values of 1.185 and 1.194 for the 1173 and 1332 keV line bands (SE, 277824 d.o.f.), and 0.665 and 0.663 for the 1173 and 1333 keV line bands (ME, 615038 d.o.f.), respectively. Note that for the low number of counts in ME spectra, χ^2 statistics does not apply. Therefore, in our model fitting approach (Sect. 3.3), we use Poissonian statistics and maximize the Poisson-likelihood function.
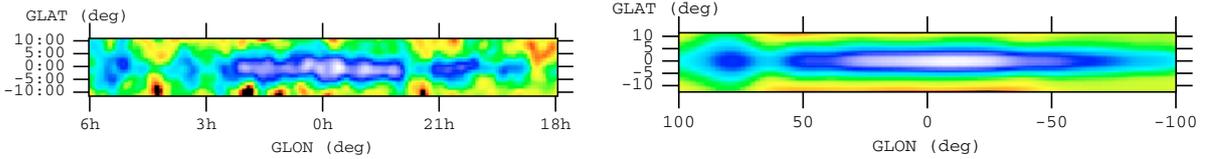
Fig. 3. Two plausible sky distribution models adopted for diffuse ^{60}Fe emission from the Galaxy. Both have been derived from COMPTEL ^{26}Al measurements (Plüschke et al. 2001; Knödlseder et al. 1999). The image obtained with the Maximum-entropy method (*left*) shows more structure, while the image derived with the Multi-resolution Expectation Maximization Method (MREM) appears smooth from its noise-filtering, accepting only image structure which is enforced by the measurements.

3.3. Model fitting and spectra

We combine above background models with a spatial model for sky emission (Fig. 3) to fit our data, allowing for adjustments of fit parameters for background and sky intensities. For this, we use a maximum-likelihood method (*spimodfit*, for more details of methods, see Strong et al. 2005) based on Poissonian statistics. We then derive per energy bin, the fitted parameter values with uncertainties, the covariance matrices, and the fitted model components. The counts per energy bin, per detector, and per pointing are fitted to the background model described in Sect. 3.2 and the assumed sky map of celestial emission (e.g., ^{26}Al distribution obtained by COMPTEL, see Fig. 3) as convolved into the domain of spectra per detector, energy bin, and pointing through the pointing sequence and the instrumental response:

$$D_{\mathrm{e,d,p}} = \sum_{m,n} A_{\mathrm{e,d,p}}^{m,n} \beta_{\mathrm{s}} I^{m,n} + \sum_{i=1}^{3} \beta_{b,i} B_{\mathrm{e,d,p}}^{i} + \delta_{\mathrm{e,d,p}}, \qquad (1)$$

where e, d, p are indices for data space dimensions: energy, detector, pointing; *m,n* indices for the sky dimensions (galactic longitude, latitude); A is the instrument response matrix, I is the intensity per pixel on the sky. Coefficients β_{s} for the sky map intensity (constant in time) and $\beta_{b,1}, \beta_{b,2}, \beta_{b,3}$ for three background intensities are derived (see Sect. 3.2 and Fig. 2; different normalizations allowed for each camera configuration of 19/18/17 functional detector elements due to failure of two Ge detectors), and the amplitude β_{s} comprises the resultant spectra of the signal from the sky. δ is the count residue after the fitting. Generally, a good fit will lead to residuals being statistically distributed around zero (see Fig. 4).

Separate fits are made for each of the Fe lines and for SE and ME, respectively. These produce four spectra of sky brightness amplitudes per energy bin. If background models are adequate, the continuum energy bands should show sky amplitudes statistically consistent with zero sky brightness. Non-zero sky brightness should show up in the form of lines with a shape conforming to the instrumental line width, possibly broader if the celestial line energy is broadened already (as had been discussed for ^{26}Al, see Diehl et al. 2006). Due to the low intensity of expected ^{60}Fe emission, we do not attempt to derive line shape information at all, and rather derive the ^{60}Fe line amplitude by fitting a Gaussian with fixed instrumental width to the *spimodfit* result spectra, determining line centroids and amplitudes in this way. From strong nearby instrumental lines, we determine that a Gaussian with a width of 2.76 keV is an adequate model for narrow lines in the regime of the ^{60}Fe lines; we use this shape to determine ^{60}Fe line parameters from the *spimodfit* result spectra. For a consistent celestial signal from ^{60}Fe, the lines should be around the ^{60}Fe decay energies of 1173 and 1333 keV and equal (within errors) in amplitudes for all four data sets.

4. Results

4.1. SPI detection of ^{60}Fe

From independently fitting the SE and ME data sets at 1 keV-wide energy bins in the energy ranges of the two lines of ^{60}Fe emission (1173 keV and 1333 keV), we obtain the four spectra from *spimodfit* (Sect. 3.3) shown in Fig. 5. Our fitted model consists of the sky intensity distribution of ^{26}Al from 9-year COMPTEL observations (Fig. 3, maximum entropy image as a standard input, Plüschke et al. 2001), together with the background model based on measurements in energy bands adjacent to the ^{60}Fe lines and on background tracers (see above). We find excess amplitudes for the celestial component in each of the four spectra.

Residual background imperfections are small except for the instrumental line at 1333 keV. The continuum flux levels are close to zero within 10^{-5} ph cm^{-2} s^{-1} rad^{-1} keV^{-1}, without apparent energy dependence, and adding a linear slope to our spectral fit function does not improve the fit[1]. The ^{69}Ge line at 1337 keV has also been eliminated rather well, though not completely. Suppression is a factor ~4 better than our previous work (Harris et al. 2005). However, this strong instrumental line still leads to a spectral signal which is recognized clearly as an artifact and thus not confused with the celestial line.

We then determine the ^{60}Fe line parameters in these spectra fitting a continuum and Gaussians representing the SPI spectral response (Sect. 2). The width of the Gaussian profiles has been fixed at 2.76 keV, the value derived from simultaneously-measured adjacent instrumental-line shapes (e.g. the instrumental line at 1107 keV). We thus obtain ^{60}Fe line positions and intensities from fitting the four spectra of Fig. 5, where the total line flux for each line in the inner Galaxy region (e.g. $-30° < l < 30°$ and $-10° < b < 10°$) is determined from the intensity of our fitted Gaussians and from the normalization of the input sky map. We present line fluxes of each of the two ^{60}Fe lines for the SE and ME data in Table 1, respectively. All line flux values are consistent within uncertainties.

A superposition of the four spectra of Fig. 5 is shown in Fig. 6. Line energies of the ^{60}Fe lines in the laboratory are 1173.23 and 1332.49 keV. For this superposition, we therefore define the zero of the relative energy axis at 1173 and 1333 keV, to derive the summed spectrum of all ^{60}Fe signals. The line flux estimated from the combined spectrum is $(4.4 \pm 0.9) \times 10^{-5}$ ph cm^{-2} s^{-1} rad^{-1}. Our significance estimate for the combined spectrum is ~4.9σ, adding uncertainties of the individual spectra in quadrature. This improves upon earlier ^{60}Fe signal reports from RHESSI (Smith 2004) and the first year of SPI data (Harris et al. 2005).

---

[1] The diffuse gamma-ray continuum emission around ^{60}Fe line energies in the inner Galaxy is ~2×10^{-6} ph cm^{-2} s^{-1} rad^{-1} keV^{-1} from COMPTEL measurements (Strong et al. 1999), which is well below the error bars of spectral counts in Fig. 5.
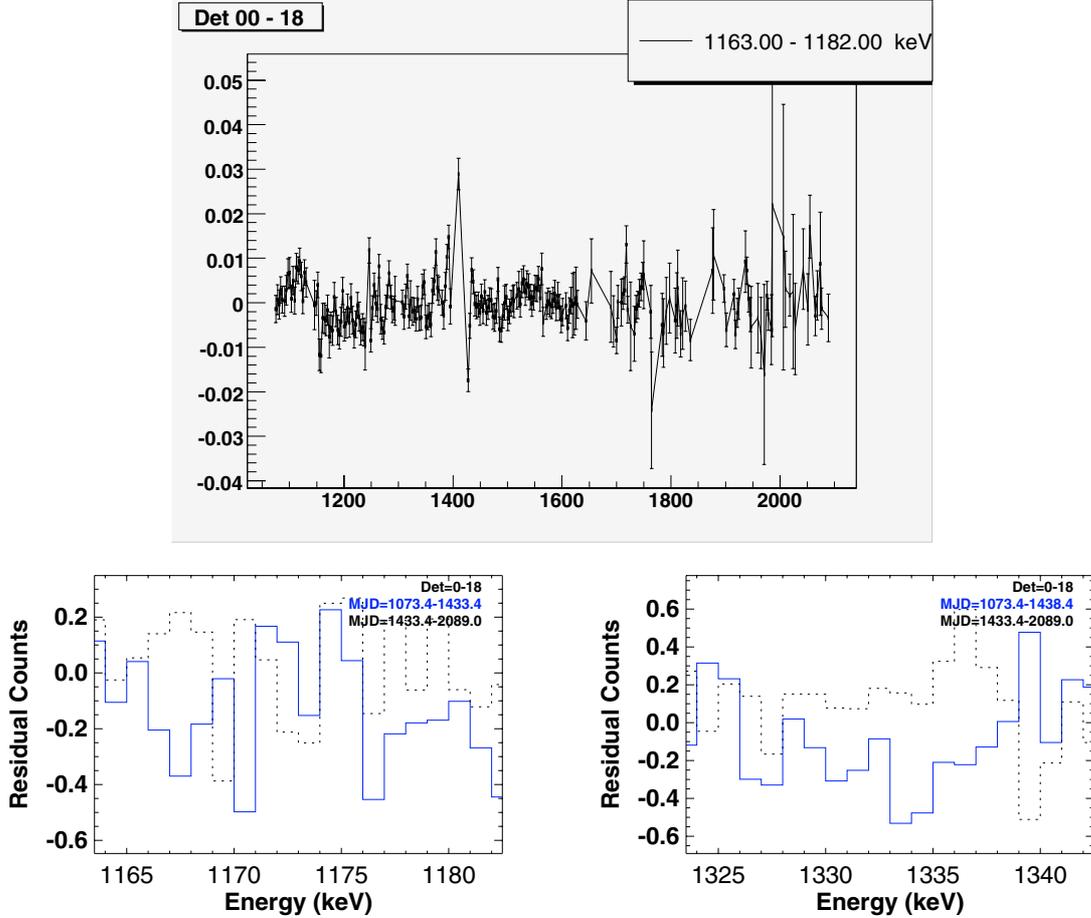
Fig. 4. Residuals of counts after fitting, in different projections. The upper figure shows the residuals versus time (days of the Julian Date, starts at 1 Jan. 2000), where counts per pointing have been re-binned into 3-day intervals for clarity (here for single events SE in the 1163–1182 keV energy band). The lower two figures present the residuals projected with the energy (SE cases for the bands around the 1173 and 1333 keV lines separately). Two different time periods are shown (dashed: first half of database; solid: second half of database). For the 1333 keV line case, because of the strong instrumental ^{69}Ge line at 1337 keV, there still exist the large residuals around 1337 keV. Residuals around zero generally confirm that our background models are adequate except for the instrumental line around 1337 keV, with χ^2/d.o.f. in model fittings (Sect. 3.3): 1.182 (SE) and 0.670 (ME) for the 1173 keV line; 1.191 (SE) and 0.667 (ME) for the 1333 keV line.

The signal of celestial ^{60}Fe is very weak, and marginally significant ($<3\sigma$) in each of our four spectra. Therefore we cannot evaluate line shape information. The lines in our spectra appear well represented by Gaussians with instrumental widths (Figs. 5 and 6), suggesting that the celestial ^{60}Fe lines are intrinsically-narrow lines. If we assume a line broadening of 1 keV, line fluxes would increase by ~6%.

4.2. ^{60}Fe and ^{26}Al

It has been argued that ^{26}Al and ^{60}Fe share at least some of the same production sites, i.e. massive stars and supernovae (e.g., Timmes et al. 1995; Limongi & Chieffi 2006). In addition both are long-lived radioactive isotopes, so we have good reasons to believe their gamma-ray distributions are similar as well. Therefore we adopt the sky distribution of ^{26}Al gamma-rays as our model for celestial ^{60}Fe gamma-ray distribution.

From our model-fitting approach (Sect. 3.3), in principle, the spectral result depends on the input sky map (also see Eq. (1)). We do not know the real distribution of ^{60}Fe sources in the Galaxy, but we need a realistic model for these sources to derive correct spectra and line intensity. As an alternative to the COMPTEL ^{26}Al maximum entropy and MREM sky maps,

we also tried a different sky map: an exponential-disk model with scale radius 4 kpc, and scale height 180 pc. This should also be a good first-order representation of ^{26}Al emission from the inner Galaxy, and but avoids the fine structure inputs from the COMPTEL image measurements which may partly arise from instrumental or analysis imperfections. We find that different input sky maps do not change the line profiles and intensities significantly (variations of the line fluxes are within 10% of the quoted values, i.e. below the uncertainties). If we use very different and scientifically implausible sky distribution models, e.g., a point source at $l = \pm 20°$, a bulge model (a Gaussian profile in the Galactic center), or a COMPTEL ^{26}Al map zeroed in the inner region of $-40° < l < 40°$, $-10° < b < 10°$, then no signals are found near the ^{60}Fe line energies.

If we hypothesize a massive-star origin for 60Fe, then the measurement of the gamma-ray flux ratio ^{60}Fe/^{26}Al is important for discussions of the astrophysical nucleosynthesis origins of the two radioactive isotopes, and the nuclear physics involved in models for their production (addressing the uncertain nuclear reaction cross sections and half-lives). For this purpose, we apply the same analysis method on the ^{26}Al data from the same observations, analyzing the 1785–1826 keV energy band (1 keV bins). We again generate a specific background model
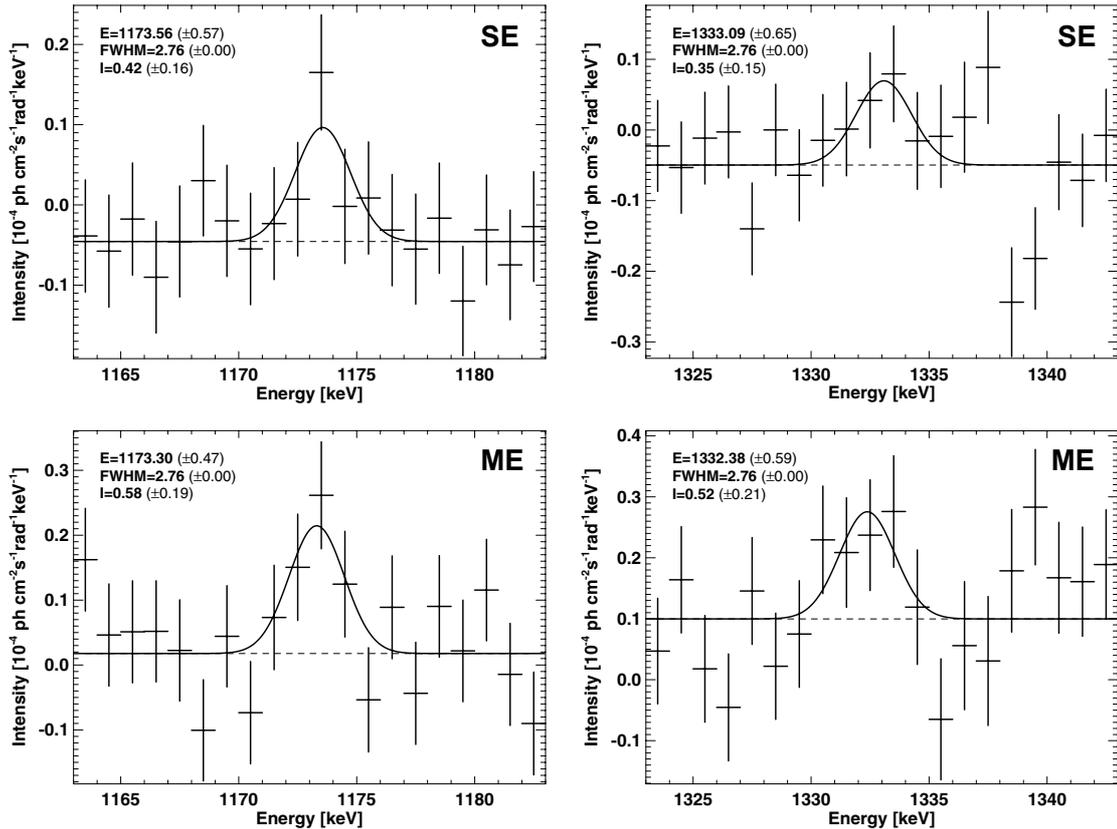
Fig. 5. The spectra of two gamma-ray lines of ^{60}Fe from the inner Galaxy: 1173 keV and 1333 keV. We have shown the results both from SE and ME databases. The data points are fitted with Gaussian profiles of fixed instrumental width (2.76 keV), and fixed continuum slope (flat), with χ^2/d.o.f. of fits: 1.06 (SE) and 1.09 (ME) for the 1173 keV line and 1.16 (SE) and 1.11 (ME) for the 1333 keV line. For the SE database, we find a line flux of $(4.2 \pm 1.6) \times 10^{-5}$ ph cm^{-2} s^{-1} rad^{-1} for the 1173 keV line and $(3.5 \pm 1.5) \times 10^{-5}$ ph cm^{-2} s^{-1} rad^{-1} for the 1333 keV line. For the ME database, the line flux is $(5.8 \pm 1.9) \times 10^{-5}$ ph cm^{-2} s^{-1} rad^{-1} for the 1173 keV line and $(5.2 \pm 2.1) \times 10^{-5}$ ph cm^{-2} s^{-1} rad^{-1} for the 1333 keV line (also see Table 1).

Table 1. ^{60}Fe intensity in the inner Galaxy.

	Flux (10^{-5} ph cm^{-2} s^{-1} rad^{-1})
1173 keV (SE)	4.2 ± 1.6
1173 keV (ME)	5.8 ± 1.9
1333 keV (SE)	3.5 ± 1.5
1333 keV (ME)	5.2 ± 2.1

(from adjacent energy bands and the GEDSAT background intensity tracer), and apply the same input sky map (the 9-year COMPTEL ^{26}Al maximum entropy map) in model fitting the SE data. This yields a flux ratio of ^{60}Fe/^{26}Al in a self-consistent way, with $F(^{60}\text{Fe})/F(^{26}\text{Al}) = (14.8 \pm 6.0)\%$. Here, the uncertainty has been estimated from the respective model-fitting uncertainties of the two SE databases. Alternatively, from the combined spectrum of ^{60}Fe lines (Fig. 6), and adopting the ^{26}Al intensity measured with SPI before ($F(^{26}\text{Al}) = (3.04 \pm 0.31) \times 10^{-4}$ ph cm^{-2} s^{-1} rad^{-1} for the inner Galaxy, see Fig. 5 of Diehl et al. 2006), we obtain $F(^{60}\text{Fe})/F(^{26}\text{Al}) = (14.5 \pm 4.0)\%$.

4.3. The Cygnus and Vela regions

The Cygnus region is one of the most active nearby star formation regions in our Galaxy. It contains a large number of massive stars and rich OB associations at a distance of 1–2 kpc (e.g. Knödlseder 2000; Le Duigou & Knödlseder 2002), and has been recognized as a prominent source of ^{26}Al with COMPTEL (Diehl et al. 1995a; Plüschke et al. 2001) and with *INTEGRAL*/SPI (Knödlseder et al. 2004). From these massive stars, ^{60}Fe gamma-rays at the 1173 keV and 1333 keV decay lines may also be expected. Since the majority of Cygnus region star-clusters are young (~3 Myr), from population synthesis studies of the massive stars in the Cygnus region it has been suggested that the ^{60}Fe production is low, consistent with the small number of recent supernova events inferred for this region ($F(1173 \text{ keV}) \sim 2 \times 10^{-6}$ ph cm^{-2} s^{-1}, see Knödlseder et al. 2002).

The Vela region in the southern sky includes even more nearby massive stars, and prominent candidate ^{26}Al sources such as the Wolf-Rayet star WR 11 in the binary system γ^2Vel at $d \sim 260$ pc (van der Hucht et al. 1997), and the core-collapse supernova remnant Vela SNR at $d \sim 250$ pc (Cha et al. 1999). 1809 keV line emission of ^{26}Al from the Vela region has been reported from COMPTEL (Diehl et al. 1995b). And this emission is not attributed to the nearby γ^2Vel source (Oberlack et al. 2000) and may be either diffuse or due to supernovae in the region. Therefore the Vela region should be a good candidate for gamma-ray line emission from ^{60}Fe.

Splitting our model sky map into independent components to fit the data, we do not see significant contributions from either region; our estimated upper limits for ^{60}Fe gamma-rays from the Cygnus ($68° < l < 92°$, $-10° < b < 14°$) and Vela ($255° < l < 273°$, $-9° < b < 9°$) regions are ~1.1×10^{-5} ph cm^{-2} s^{-1} (2σ). More detailed studies are in progress (Schanne et al. 2007; Martin et al., in preparation).
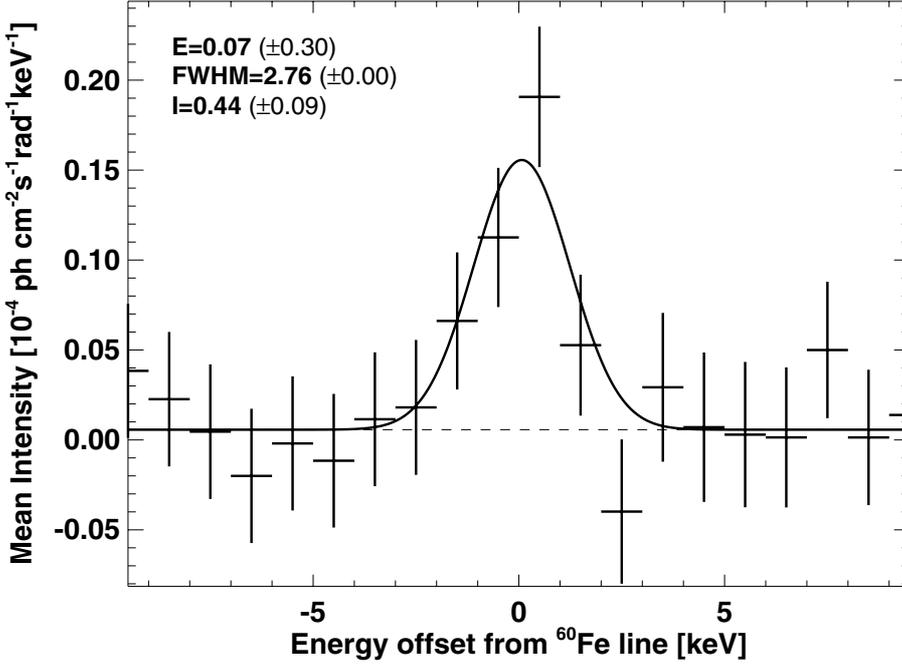
Fig. 6. The combined spectrum of the ^{60}Fe signal in the inner Galaxy, superimposing the four spectra of Fig. 2. In the laboratory, the line energies are 1173.23 and 1332.49 keV; here superimposed bins are zero at 1173 and 1333 keV. We find a detection significance of 4.9σ. The solid line represents a fitted Gaussian profile of fixed instrumental width (2.76 keV), and a flat continuum. The average line flux is estimated as $(4.4 \pm 0.9) \times 10^{-5}$ ph cm^{-2} s^{-1} rad^{-1}.
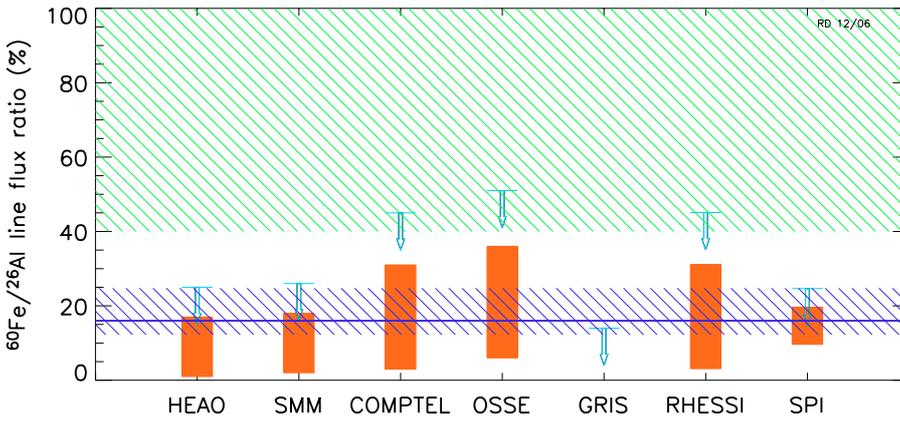

Fig. 7. Flux ratio of the gamma-ray lines from the two long-lived radioactive isotopes ^{60}Fe/^{26}Al from several observations, including our SPI result (also see Table 2), with upper limits shown at 2σ for all reported values, and comparison with the recent theoretical estimates (the upper hatched region from Prantzos 2004; the horizontal line taken from Timmes et al. 1995; the lower hatched region, see Limongi & Chieffi 2006). Our present work finds the line flux ratio to be (14.8 ± 6.0)%. Note that the primary instrument results on ^{60}Fe is compromised in the figure by different and uncertain ^{26}Al fluxes used for the ^{60}Fe/^{26}Al ratio (see Table 2 for details).

5. Summary and discussions

We report the detection of ^{60}Fe decay gamma-ray lines in the Galaxy from 2.5 years of SPI observations. With our new measurements we detect both the 1173 keV and 1333 keV line of ^{60}Fe from SPI single and multiple-detector events. Combining our four spectra from independent model fits we obtain an ^{60}Fe signal from the Galaxy with a significance of 4.9σ. This improves upon our previous measurements (see Harris et al. 2005). The average ^{60}Fe line flux from the inner Galaxy region is $(4.4 \pm 0.9) \times 10^{-5}$ ph cm^{-2} s^{-1} rad^{-1}, assuming intrinsically narrow lines and a sky distribution equal to that of ^{26}Al as measured by COMPTEL (Plüschke et al. 2001). From the same observations and analysis procedure applied to ^{26}Al, we find a flux ratio of ^{60}Fe/^{26}Al of (14.8 ± 6.0)%. The ^{60}Fe signals are too weak to determine line shape details; it appears that a Gaussian with the width of the instrumental resolution can fit the data well. This would imply that broadening of ^{60}Fe lines from astrophysical processes is not significant; most of the ^{60}Fe may be distributed in a rather normal interstellar medium with turbulent velocities below ~300 km s^{-1}. In order to investigate the variations over the Galaxy, we search for ^{60}Fe emission from the Cygnus and Vela regions, and do not find ^{60}Fe signals.

Table 2. Different measurements of ^{60}Fe flux in units of 10^{-5} ph cm^{-2} s^{-1} rad^{-1} from the inner Galaxy and ^{60}Fe/^{26}Al flux ratio.

Experiments	^{60}Fe flux	^{60}Fe/^{26}Al	References
HEAO-3	5.3 ± 4.3	0.09 ± 0.08	Mahoney et al. (1982)
SMM	2.9 ± 2.5	0.1 ± 0.08	Leising & Share (1994)
OSSE	6.3 ± 4.5	0.21 ± 0.15	Harris et al. (1997)
COMPTEL	6.7 ± 5.4	0.17 ± 0.135	Diehl et al. (1997)
GRIS	<6.8(2σ)	<0.14(2σ)	Naya et al. (1998)
RHESSI	3.6 ± 1.4	0.17 ± 0.13	Smith (2004)
SPI	4.4 ± 0.9	0.148 ± 0.06	this work

Many experiments and efforts were made (see Table 2 and Fig. 7) to measure the ^{60}Fe gamma-ray emission that was predicted by theory – we now provide the most significant detection to date. In Fig. 7, we show the previous constraints on the flux ratio of ^{60}Fe/^{26}Al together with the result of this work, and compare the observational results with different theoretical predictions. The earliest observational limit was given from HEAO-3, $F(^{60}$Fe$)/F(^{26}$Al$) = 0.09 \pm 0.08$, an upper limit being 0.27 (Mahoney et al. 1982) (in Fig. 7, we chose to give limits at 2σ for all reported values below a significance of 3σ). Another limit

was obtained with the SMM Gamma-Ray Spectrometer, a flux ratio of 0.1 ± 0.08, the upper limit being ~0.27 (Leising & Share 1994). OSSE aboard the COMPTON Observatory gave a flux ratio of 0.21 ± 0.15, and the upper limit is ~0.51 (Harris et al. 1994, 1997). COMPTEL aboard the COMPTON Observatory also found ^{60}Fe gamma-rays, and reported a flux ratio value of ^{60}Fe/^{26}Al of 0.17 ± 0.135, which translates into an upper limit ~0.44 (Diehl et al. 1997). The Gamma-Ray Imaging Spectrometer (GRIS) reported an upper limit for the ratio of <0.14 (2σ, Naya et al. 1998). RHESSI then reported the first detection of ^{60}Fe gamma-ray lines, and gave a flux ratio 0.17 ± 0.13 with two-year data (Smith 2004). The first year data of SPI gave a flux ratio 0.11 ± 0.07 (Harris et al. 2005), and the present analysis of the 2.5-year SPI data finds a flux ratio 0.148 ± 0.06.

Theoretical predictions of the ratio of ^{60}Fe/^{26}Al have undergone some changes since Timmes et al. (1995) published the first detailed theoretical prediction. In their paper, they combine a model for ^{26}Al and ^{60}Fe nucleosynthesis in supernova explosions with a model of chemical evolution, to predict that the steady production rates are (2.0 ± 1.0) $M_\odot$ Myr^{-1} for ^{26}Al, and (0.75 ± 0.4) $M_\odot$ Myr^{-1} for ^{60}Fe, which corresponds to a gamma-ray flux ratio $F(^{60}$Fe$)/F(^{26}$Al$) = 0.16 \pm 0.12$. This prediction would be consistent with our present measurements. Since 2002, theoreticians have improved various aspects of the stellar-evolution models, including improved stellar wind models and the corresponding mass loss effects on stellar structure and evolution, of mixing effects from rotation, and also updated nuclear cross sections in the nucleosynthesis parts of the models. As a result, predicted flux ratios ^{60}Fe/^{26}Al rather fell into the range 0.8 ± 0.4 (see Prantzos 2004, based on, e.g. Rauscher et al. 2002; Limongi & Chieffi 2003) – such high values would be inconsistent with several observational limits and our SPI result (but see Woosley & Heger 2007 for comments on nuclear reaction rate updates). Recently, new calculations of ^{26}Al and ^{60}Fe yields from massive stars of solar metallicity have been presented (Limongi & Chieffi 2006; Heger & Woosley 2007). Limongi & Chieffi (2006) combined their individual yields, using a standard stellar-mass distribution function, to produce an estimate of the ^{60}Fe/^{26}Al gamma-ray flux ratio expected from massive stars. Their calculations yield again a lower prediction for the ^{60}Fe/^{26}Al flux ratio of 0.185 ± 0.0625, which is again consistent with the observational constraints (see Fig. 7).

In summary, uncertainties still exist, both in models and measurements of ^{60}Fe. On the theory side, stellar evolution in late stages is complex, nuclear reactions include neutron capture on unstable Fe isotopes, and explosive nucleosynthesis adds yet another complex ingredient. On the experimental side, cosmic ray induced ^{60}Co radioactivity in the instrument and spacecraft and the limitations of spatial resolutions and sensitivity are issues reflected in the substantial uncertainties in experimental values. With more *INTEGRAL*/SPI data to come, and also with the development of next-generation gamma-ray spectrometers/telescopes, gamma-ray observations hopefully can help with an independent view on the astrophysical model components.

References

Attie, D., Cordier, B., Gros, M., et al. 2003, A&A, 411, L71
Cha, A. N., Sembach, K. R., Danks, A. C., et al. 1999, ApJ, 515, L25
Chieffi, A., & Limongi, M. 2004, ApJ, 608, 405
Courvoisier, T. J. L., Walter, R., Beckmann, V., et al. 2003, A&A, 411, L53
Diehl, R., Dupraz, C., Bennett, K., et al. 1995a, A&A, 298, 445
Diehl, R., Bennett, K., Bloemen, H., et al. 1995b, A&A, 298, L25
Diehl, R., Wessolowski, U., Oberlack, U., et al. 1997, AIPC, 410, 1109
Diehl, R., Halloin, H., Kretschmer, K., et al. 2006, A&A, 449, 1025
Halloin, H., et al. 2007, A&A, in preparation
Hajdas, W., Bühler, P., Eggel, C., et al. 2003, A&A, 411, L43
Harris, M. J., Purcell, W. R., Grabelsky, D. A., et al. 1994, AAS, 184, 6502
Harris, M. J., Purcell, W. R., McNaron-Brown, K., et al. 1997, AIPC, 410, 1079
Harris, M. J., Knödlseder, J., Jean, P., et al. 2005, A&A, 433, L49
Iyudin, A. F., Diehl, R., Bloemen, H., et al. 1994, A&A, 284, L1
Iyudin, A. F., Bennett, K., Bloemen, H., et al. 1995, A&A, 300, 422
Knödlseder, J. 2000, A&A, 360, 539
Knödlseder, J., Bennett, K., Bloemen, H., et al. 1999, A&A, 344, 68
Knödlseder, J., Cerviño, M., Le Duigou, J.-M., et al. 2002, A&A, 390, 945
Knödlseder, J., Valsesia, M., Allain, M., et al. 2004, ESA-SP, 552, 33
Kurfess, J. D., Johnson, W. N., Kinzer, R. L., et al. 1992, ApJ, 399, 137
Le Duigou, J.-M., & Knödlseder, J. 2002, A&A, 392, 869
Leising, M. D., & Share, G. H. 1994, 424, 200
Leleux, P., Albernhe, F., Borrel, V., et al. 2003, A&A, 411, L85
Limongi, M., & Chieffi, A. 2003, ApJ, 592, 404
Limongi, M., & Chieffi, A. 2006, ApJ, 647, 483
Mahoney, W. A., Ling, J. C., Jacobson, A. S., & Lingerfelter, R. E. 1982, ApJ, 262, 742
Matz, S. M., Share, G. H., Leising, M. D., Chupp, E. L., & Vestrand, W. T. 1988, Nature, 331, 416
Naya, J. E., Barthelmy, S. D., Bartlett, L. M., et al. 1998, ApJ, 499, L169
Oberlack, U., Wessolowski, U., Diehl, R., et al. 2000, A&A, 353, 715
Plüschke, S., Diehl, R., Schönfelder, V., et al. 2001, ESA-SP, 459, 55
Prantzos, N. 2004, A&A, 420, 1033
Rauscher, T., Herger, A., Hoffman, R. D., & Woosley, S. E. 2002, ApJ, 576, 323
Renaud, M., Lebrun, F., Ballet, J., et al. 2004, ESA-SP, 552, 81
Renaud, M., Vink, J., Decourchelle, A., et al. 2006, ApJ, 647, L41
Roques, J. P., Schanne, S., von Kienlin, A., et al. 2003, A&A, 411, L91
Schanne, et al. 2007, the Moscow *INTEGRAL* worshop, ESA-SP, in press
Sizun, P., et al. 2007, A&A, in preparation
Smith, D. M. 2004, ESA-SP, 552, 45
Strong, A. W., Bloemen, H., Diehl, R., Hermsen, W., & Schönfelder, V. 1999, Astrophys. Lett. Comm., 39, 209
Strong, A. W., Diehl, R., Halloin, H., et al. 2005, A&A, 444, 495
The, L. S., Clayton, D. D., Diehl, R., et al. 2006, A&A, 450, 1037
Timmes, F. X., Woosley, S. E., Hartmann, D. H., et al. 1995, ApJ, 449, 204
van der Hucht, K. A., Schrijver, H., Stenholm, B., et al. 1997, New Astron., 2, 245
Weidenspointner, G., Kiener, J., Gros, M., et al. 2003, A&A, 411, L113
Woosley, S. E. 1997, ApJ, 476, 801
Woosley, S. E., & Heger, A. 2007, APS 2005 Bethe Prize Lectures, Phys. Rep., in press [arXiv:astro-ph/0702176]